15. Saijo Y, Tanaka M, Okawai H, Dunn F. The ultrasonic properties of gastric cancer tissues obtained with a scanning acoustic microscope system. Ultrasound Med Biol 1991;17:709-14.
16. Saijo Y, Tanaka M, Okawai H, Sasaki H, Nitta S-I, Dunn F. Ultrasonic tissue characterization of infarcted myocardium by scanning acoustic microscopy. Ultrasound Med Biol 1997;23:77-85.
17. Saijo Y, Sasaki H, Okawai H, Nitta S-I, Tanaka M. Acoustic properties of atherosclerosis of human aorta obtained with high-frequency ultrasound. Ultrasound Med Biol 1998;24:1061-4.
18. Saijo Y, Chubachi N. Microscopy. Ultrasound Med Biol 2000; 26(Suppl 1):S30-2.
19. Saijo Y, Jorgensen C S, Falk E. Ultrasonic tissue characterization of collagen in lipid-rich plaques in apoE-deficient mice. Atherosclerosis 2001;158:289-95.
20. Sano H, Ishii H, Backman DS, Brunet JA, Trudel G, Uhthoff HK. Structural disorders at the supraspinatus tendon insertion—their relation to tensile strength. J Bone Joint Surg Br 1998;80B:720-5.
21. Sano H, Saijo Y, Kokubun S. Material properties of the supraspinatus tendon at its insertion—a measurement with the scanning acoustic microscopy. J Musculoskeletal Res 2004;8:29-34.
22. Sano H, Wakabayashi I, Itoi E. Stress distribution in the supraspinatus tendon with partial-thickness tears: an analysis using two-dimensional finite element model. J Shoulder Elbow Surg 2006; 15:100-5.
23. Sasaki H, Saijo Y, Tanaka M, et al. Influence of tissue preparation on the high-frequency acoustic properties of normal kidney tissue. Ultrasound Med Biol 1996;22:1261-5.
24. Soslowsky LJ, Carpenter JE, DeBano CM, Banerji I, Moalli MR. Development and use of an animal model for investigations on rotator cuff disease. J Shoulder Elbow Surg 1996;5:383-92.
25. Turner CH, Rho J, Takano Y, Tsui TY, Pharr GM. The elastic properties of trabecular and cortical bone tissues are similar: results from two microscopic measurement techniques. J Biomechanics 1999;32:437-41.
26. Uhthoff HK, Sano, H. Pathology of failure of the rotator cuff tendon. Orthop Clin North Am 1997;28:31-41
27. Wakabayashi I, Itoi E, Sano H, et al. Mechanical environment of the supraspinatus tendon: a two-dimensional finite element model analysis. J Shoulder Elbow Surg 2003;12:612-7.

Upsala J Med Sci 111 (3): 303–313, 2006

Increased Elasticity of Capsule After Immobilization in a Rat Knee Experimental Model Assessed by Scanning Acoustic Microscopy

Yoshihiro Hagiwara[1]*, Yoshifumi Saijo[2], Eiichi Chimoto1, Hirotoshi Akita[3], Yasuyuki Sasano[3], Fujio Matsumoto[1], Shoichi Kokubun[1]

[1]*Department of Orthopaedic Surgery, Tohoku University Graduate School of Medicine, Sendai, 980-8574, Japan*
[2]*Department of Medical Engineering and Cardiology, Institute of Development, Aging and Cancer, Tohoku University, Sendai 980-8575, Japan*
[3]*Division of Craniofacial Development and Regeneration, Tohoku University Graduate School of Dentistry, Sendai, Japan*

Abstract

Objectives: The mechanical property of immobilized joints is not well understood. The present study was designed to investigate the tissue elasticity of the anterior and posterior synovial membrane (SM) in a rat immobilized knee model using scanning acoustic microscopy (SAM). Moreover, the structural characteristics of the SM after immobilization were examined by transmission electron microscopy (TEM).

Methods: Thirty rats had their knee joints immobilized with a plate and metal screws. The rats were fixed at 1, 2, 4, 8 and 16 weeks after surgery and the knee joints were sectioned sagittally for SAM. Selected specimens were processed for TEM. A new concept SAM using a single pulsed wave instead of continuous waves was applied to measure the sound speed of the anterior and posterior SM, comparing it with the corresponding light microscopic images.

Results: The sound speed of the posterior SM increased significantly in the 8- and 16-week experimental group compared with that in the control group. The sound speed of the anterior SM showed no statistical difference between the experimental and the control groups at any period of immobilization. The posterior SM of the experimental group was different from that of the control group in the ultrastructural characteristics of extracellular matrices.

Conclusions: Our data suggest that the increased elasticity and structural changes of the posterior SM are one of the main causes of limited extension after a long period of immobilization in flexion using SAM, which is a powerful tool for evaluating the elasticity of targeted tissues.

Introduction

Joint contracture is defined as a decrease in both active and passive ranges of motion (ROM) after immobilization. The decreased ROM limits the activity of daily living in various aspects. Immobilization, which is a major cause of joint contracture, is beneficial for decreasing pain caused by trauma and preventing the joint from damage in the acute phase of arthritis such as pyogenic and rheumatoid arthritis [1–3]. Even by extensive rehabilitation or surgical treatment, however, it is difficult to regain the full ROM in an established joint contracture after a long period of immobilization [4,5].

Received 17 February 2006
Accepted 21 March 2006

The components of joint contracture after immobilization are classified into arthrogenic and myogenic ones. The arthrogenic components are lesions of bone, ligaments, capsule and synovial membrane (SM), while the myogenic components are lesions of muscle, tendon and fascia [6,7]. Some investigators have attributed contracture to myogenic causes (8), while others attributed it to arthrogenic causes [4,7,9–13]. It is difficult to evaluate such contradictory reports because different animal species and methods were used in their immobilization experiments. Among the arthrogenic components, the stiffness of the capsule and SM through synovial atrophy, retraction, fibrosis, and adhesion may contribute to the limited ROM [1,7,8,10,14–17]. Though increased elasticity of the capsule or SM has been suggested to be a cause of joint contracture [18], it is not known how the elasticity and the structural characteristics of extracellular matrices are affected by immobilization.

A scanning acoustic microscopy (SAM) using continuous waves characterize biological tissues by determining the elastic parameters based on the sound speed [19]. Recent studies on infarcted myocardium [20], atherosclerosis of aorta [21] and carotid arterial plaques [22] have shown that the acoustic properties reflect the collagen types. In the present study, we applied a new concept SAM using single pulsed wave, which can make total time for calculation significantly shorter, to examine the elasticity of the anterior and posterior SM (synovial intima and subintima) in the course of knee joint immobilization in a rat experimental model.

Material and Methods

Animals. The protocol for this experiment was approved by the Animal Research Committee of Tohoku University. Adult male Sprague-Dawley rats weighing from 380 to 400 g were used. Their knee joints were immobilized at 145° in flexion by rigid internal but extra-articular fixation for various periods (1, 2, 4, 8 and 16 weeks) according to a previously described method (1). The left and right hind legs were immobilized alternately to avoid potential systematic side differences. The surgery was performed under anesthesia with sodium pentobarbital (50 mg/kg) administered intraperitoneally. A rigid plastic plate (POM-N, Senko Med. Co., Japan) implanted subcutaneously joined the proximal femur and the distal tibia away from the knee joint and was solidly held in place with one metal screw (Stainless Steel, Morris, J. I., Co., USA) at each end. The knee joint capsule and the joint itself were untouched. Postoperative analgesia with buprenorphine (0.05 mg/kg) was injected subcutaneously. Sham operated animals had holes drilled in the femur and tibia and screws inserted but none of them were plated. The animals were allowed unlimited activity and free access to water and food. The immobilized animals and the sham operated animals made up the experimental groups and the control groups, respectively. Thirty rats (1, 2, 4, 8 and 16 weeks) were prepared. Each group was composed of 6 experimental and 5 control animals.

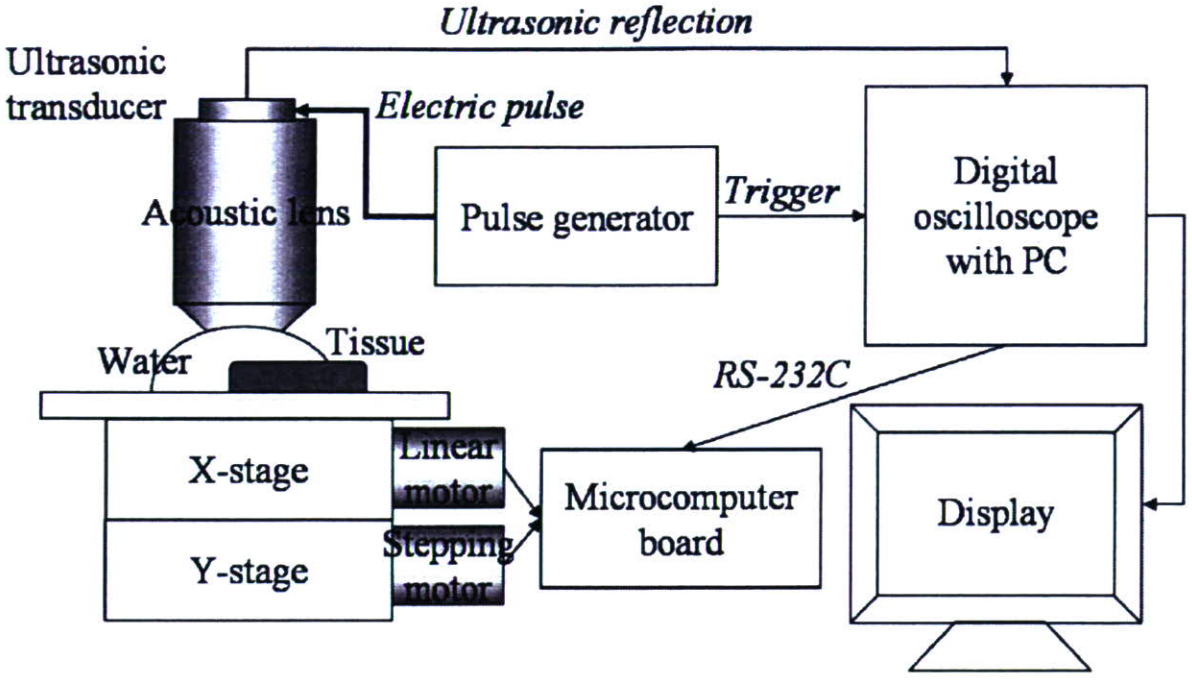

Figure 1. Schematic illustration of a new concept scanning acoustic microscopy (SAM). A new concept SAM can make total time for calculation significantly shorter than a conventional SAM by using a single pulsed wave instead of continuous waves.

Tissue preparation. The rats were anesthetized and fixed with 4% paraformaldehyde in 0.1M phosphate-buffer, pH7.4 by perfusion through the aorta. The knee joints were resected and kept in the same fixative overnight at 4C°. The fixed specimens were decalcified in 10% EDTA in 0.01M phosphate-buffer, pH7.4 for 1–2 months at 4C°. After dehydration through a graded series of ethanol solutions, the specimens were embedded in paraffin. The embedded tissue was cut into 5-μm thick sagittal sections from the medial to the lateral side of the joint. Standardized serial sections of the medial midcondylar region of the knee were made.

The serial sections were prepared for hematoxylin-eosin stain to observe the histological appearance of SM after immobilization.

Scanning acoustic microscopy. Our SAM consists of five parts: 1) ultrasonic transducer, 2) pulse generator, 3) digital oscilloscope with PC, 4) microcomputer board and 5) display unit (Figure 1). A single pulsed ultrasound with 5 ns pulse width was emitted and received by the same transducer above the specimen. The aperture diameter of the transducer was 1.2 mm and the focal length was 1.5 mm. The central frequency was 80 MHz and the pulse repetition rate was 10 kHz. Considering the focal distance and the sectional area of the transducer, the diameter of the focal spot was estimated as 20 μm at 80 MHz. Distilled water was used as the coupling medium between the transducer and the specimen. The reflections from the tissue surface and from interface between the tissue and the glass were received by the transducer and were introduced into a digital oscilloscope (Tektronics TDS 5052,

USA). The frequency range was 300 MHz and the sampling rate was 2.5 GS/s. Four pulse responses at the same point were averaged in the oscilloscope in order to reduce random noise.

The transducer was mounted on an X–Y stage with a microcomputer board that was driven by the computer installed in the digital oscilloscope through an RS-232C. The X-scan was driven by a linear servo-motor and the Y-scan was driven by a stepping motor. Finally, two-dimensional distributions of the ultrasonic intensity, sound speed and thickness of the 2.4 by 2.4 mm specimen area were visualized with 300 by 300 pixels. The total scanning time was 121 sec.

Signal analysis. The reflected waveform comprises two reflections at the surface and the interface between the tissue and the glass. The thickness and sound speed were calculated by Fourier-transforming the waveform [19].

Image analysis. Normal light microscopic images corresponding to the stored acoustic images were captured (DMLB 100 HC light microscope, LEICA Wetzlar, Germany). A region of analysis by SAM was set in the anterior and posterior SM each in each section (Figure 2). In the region, the sound speed of SM, excluding meniscus, bone and cartilage, was calculated with a gray scale SAM images using commercially available image analysis software (PhotoShop 6.0, Adobe Systems Inc., San Jose, CA) (Figure 4). SAM images with a gradation color scale were also produced for clear visualization of the sound speed. The optical and acoustic images were compared to ensure morphological congruence in the analysis.

Transmission electron microscopy. The posterior SM of 8-week experimental and control groups were fixed with a mixture of 0.04% glutaraldehyde and 4.0% paraformaldehyde in 0.1M phosphate-buffered saline, pH 7.4, at 4C° into the intra-articular space for rapid fixation. The skin around the knee was excised and the posterior SM was immersed with the same fixative for 1h at 4C°. After washed thoroughly with Dulbecco's PBS to remove the fixative, the tissue was cut with a razor blade into pieces and post-fixed with 2% buffered osmium tetroxide. The tissues were stained en bloc in aqueous uranyl acetate solution, dehydrated through a graded series of ethanol solutions and embedded in EPON 812 resin (TAAB Laboratory Equipment Ltd). Ultrathin resin sections of the specimens were mounted on copper, counterstained with uranyl acetate and Reynold's lead citrate solution, then observed with a Hitachi H-9000 electron microscope [23].

Statistics. All data were expressed as the mean ± SD. The statistical significance of difference in the results was evaluated by unpaired analysis of variance, and P values were calculated by Tukey's method. A P value less than 0.05 was considered statistically significant.

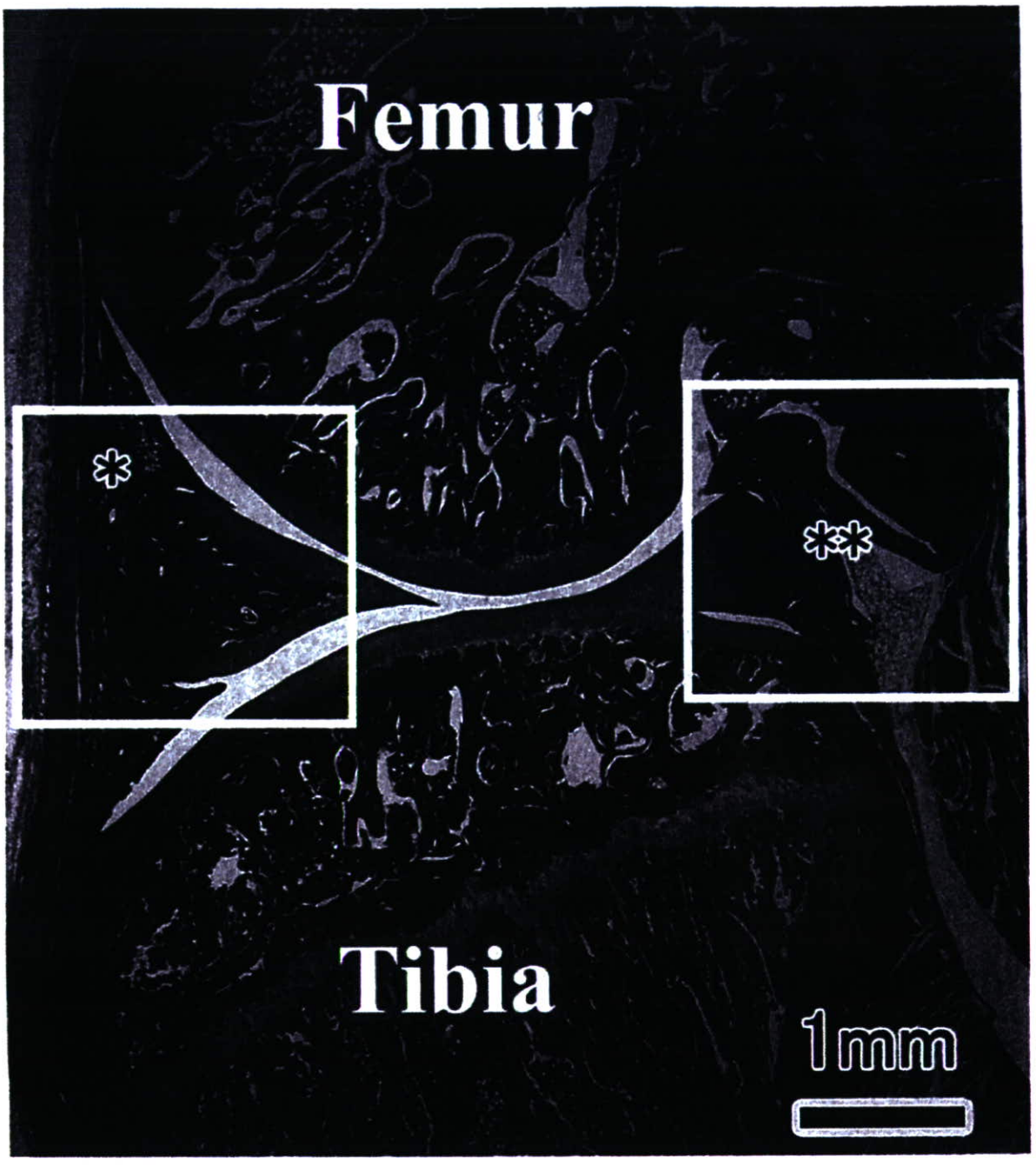

Figure 2. Microphotograph of a sagittal section in the medial midcondylar region of a rat knee. Squares indicate regions of analysis by scanning acoustic microscopy in the anterior(＊) and posterior(＊＊) synovial membrane. (Original magnification × 10, hematoxylin-eosin stain)

Results

SAM examination. The gradation color images of the posterior SM in the experimental group differed from those in the control group (Figure 3). The posterior SM was composed of low sound speed areas (black to blue) in 2-week immobilization (Figure 3A). The low sound speed area decreased and high sound speed areas (yellow to red) gradually increased in the posterior SM of the experimental group

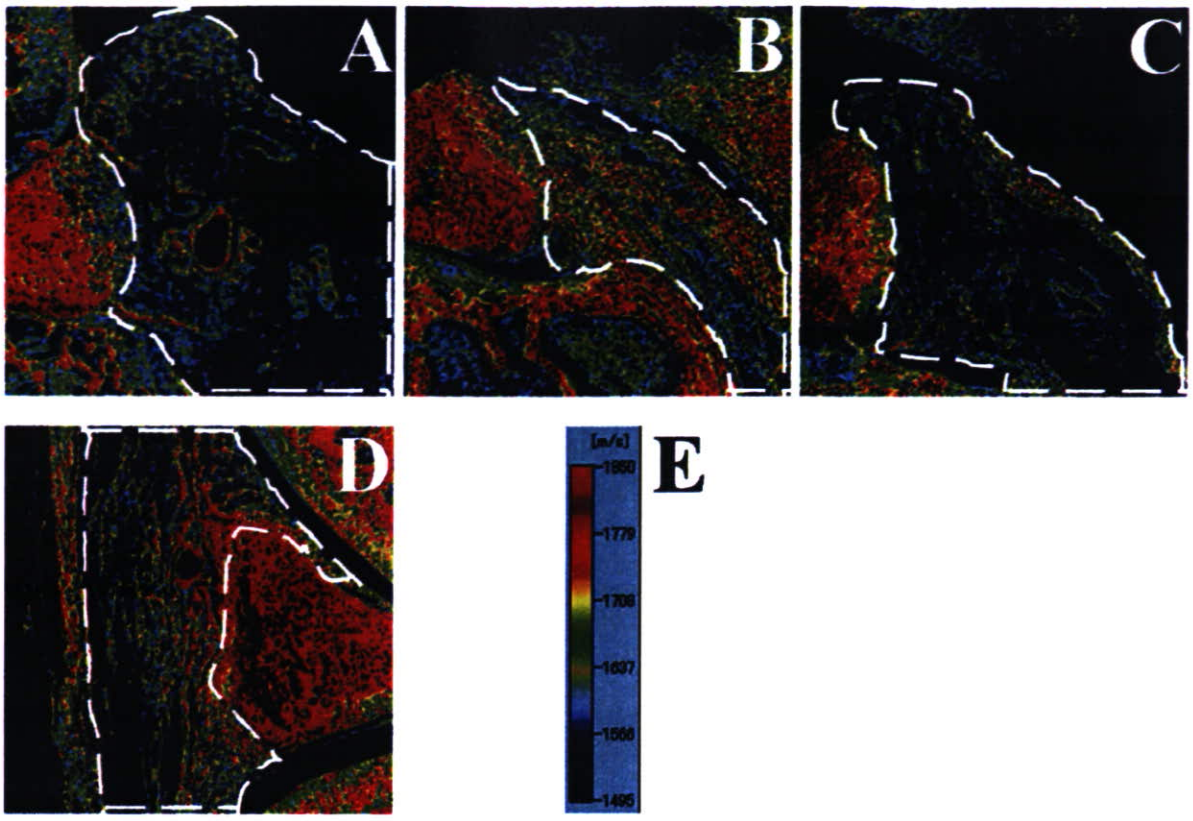

Figure 3. Gradation color images of scanning acoustic microscopy in the posterior and the anterior synovial membrane (SM). **A**, 2-week immobilization group (posterior). **B**, 16-week immobilization group (posterior). **C**, a representative of the control groups (posterior, 16-week). **D**, a representative of the control group (anterior, 16-week). **E**, gradation color table. Most low sound speed areas (black to blue) were replaced by high sound speed area (yellow to red) over time in the posterior experimental group. The posterior SM in the control groups remained entirely black to blue throughout the duration. The anterior SM was similar in the experimental and control group irrespective of the immobilization periods. Regions enclosed with a dotted line indicate the SM for calculation.

with time (Figure 3B). The posterior SM remained same in all the control groups (Figure 3C).

The anterior SM was similar in all the experimental and control groups irrespective of immobilization periods (Figure 3D).

The sound speed of the posterior SM is shown in Figure 4. There was no statistical difference between the experimental and the control groups in 1-, 2- or 4-week immobilization (1w: 1560 m/s$\pm$18.7 m/s vs. 1543 m/s$\pm$16.3 m/s; $p = 0.152$, 2w: 1552 m/s$\pm$26.0m/s vs. 1535 m/s$\pm$8.17 m/s; $p = 0.207$, 4w: 1551 m/s$\pm$4.01 m/s vs. 1553 m/s$\pm$13.3 m/s; $p = 0.698$). In 8- and 16-week immobilization, however, the sound speed in the experimental group was significantly higher than that in the control group (8w: 1546 m/s$\pm$18.7 m/s vs. 1646 m/s$\pm$11.8 m/s; $p = 6.69 \times 10^{-6}$, 16w: 1568 m/s$\pm$26.5 m/s vs. 1677 m/s$\pm$32.8 m/s; $p = 1.06 \times 10^{-4}$) (Figure 4A). There was no statistical difference in the anterior SM in all the experimental and the control groups at any period of immobilization (1w: 1563 m/s$\pm$22.7 m/s vs. 1556 m/s$\pm$13.8 m/s; $p = 0.545$, 2w: 1562 m/s$\pm$12.4 m/s vs. 1565 m/s$\pm$11.4 m/s; $p = 0.74$, 4w: 1559 m/s$\pm$10.1 m/s vs. 1554 m/s$\pm$30.4 m/s; $p = 0.745$, 8w: 1550m/

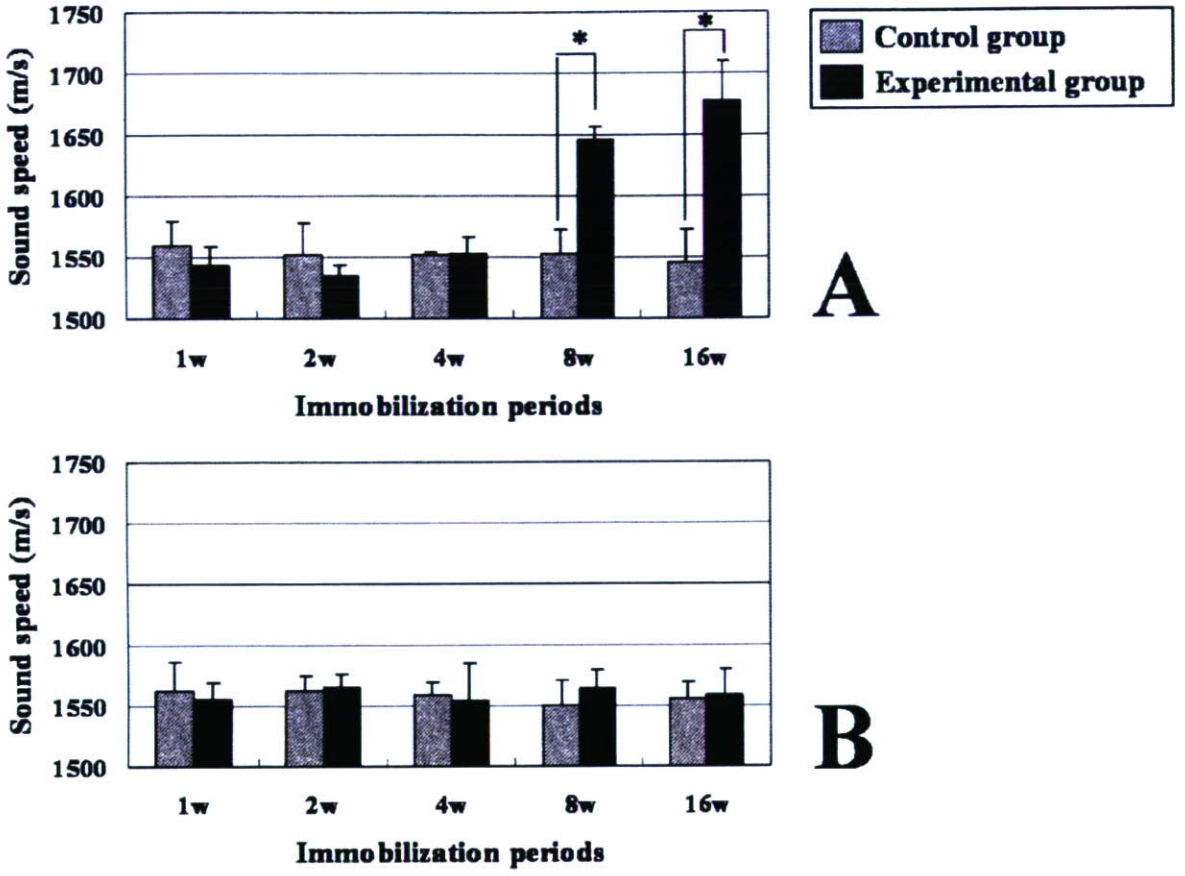

Figure 4. Sound speed changes of the posterior and the anterior synovial membrane (SM). **A**, the posterior SM. **B**, the anterior SM. In the posterior SM, significant difference of sound speed is seen in 8- and 16-week immobilization. There was no statistical difference at any period of immobilization in the anterior SM. solid bars = experimental groups, shaded bars = control groups. Values are the mean ± SD. * = $P < 0.005$ versus control, by Tukey's method.

s ± 20.5 m/s vs. 1564 m/s ± 15.3 m/s; p = 0.263, 16w: 1556 m/s ± 14.1 m/s vs. 1558 m/s ± 22.6 m/s; p = 0.846) (Figure 4B).

TEM examination. In the experimental group, the space among collagen bundles and cells were occupied with the high density matrix, which fills the interspace of collagen microfibrils within the collagen bundle. In contrast, the high density matrix surrounding cells, collagen bundles and fibrils were scarce in the control group (Figure 5).

Discussion

The arthrogenic component has been considered as an important factor of joint contracture after immobilization (1,7,8,10,14–18). In a study using a rabbit knee contracture model, the mechanical characteristics were quantified by a torque-angular displacement diagram [18]. Knees in 9-week immobilization in flexion showed a significantly larger torque in extension in the experimental group than in the control

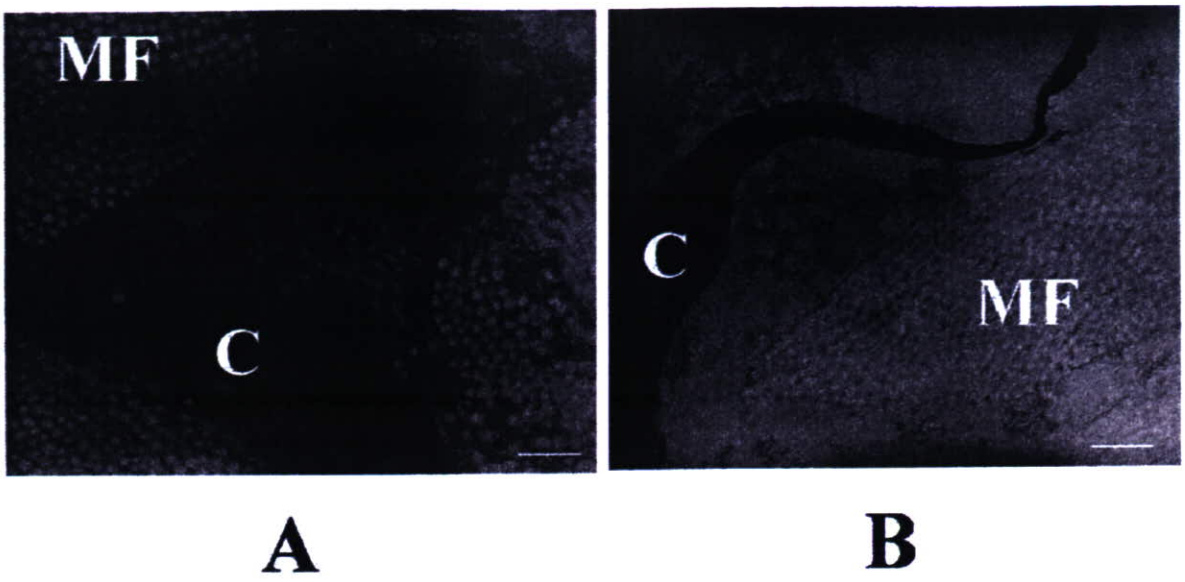

Figure 5. Structural characteristics of the posterior synovial membrane (SM). **A**, 8-week experimental group. **B**, 8-week control group. Compared with the control group, the space among collagen bundles and cells were occupied with the high density matrix, which fills the interspace of collagen microfibrils within the collagen bundle in the experimental group. ***C***, cell; ***MF***, microfibrils. (Original magnification × 360,000, scale bar = 0.5 μm).

group even after total extra-articular myotomies. In the same rat model as ours in the present study but immobilized up to 32 weeks, ROM in extension still remained restricted even after total extra-articular myotomies [7]. In canine glenohumeral joint immobilized up to 16 weeks, the intra-articular pressure rose higher by injection of Hypaque contrast medium and the filling volume was smaller compared with the control group at a rupture of the capsule [24]. These studies suggest that among the arthogenic components, the capsule and SM may mostly contribute to production of joint contracture.

Connective tissue proliferation in the SM and its adhesion to articular cartilage in the intra-articular space has been considered as pathological features of contracture after immobilization [25–29]. But conflicting studies with it have been reported. No intra-articular connective tissue proliferation occurred after immobilization [1,30–32]. No contact between the connective tissue and articular cartilage was observed [32]. In the same rat model as ours in the present study but immobilized up to 32 weeks, the decrease in the synovial intima length was observed after 4-week immobilization [1]. This study concluded that mutual adhesions of synovial villi rather than the connective tissue proliferation were the major pathophysiological changes leading to contracture. Further, the decrease of the synovial intima length was reported to be greater in the posterior SM than in the anterior SM in the same model as ours in the present study [1]. It may be explained as earlier mutual adhesion of synovial villi in the posterior SM under less tension with the knee immobilized in flexion.

Connective tissue response after immobilization is important to understand the mechanism of the increased elasticity of the posterior SM. Some suggestions con-

cern changes in the biochemical composition of periarticular fibrous connective tissue (e.g. patellar tendon, ligament and joint capsule) after immobilization. The notable change was a reduction of water and glycosaminoglycans without decreased collagen mass [9,18,32,33]. These changes were expected to alter plasticity and pliability of connective tissue matrices and to reduce lubrication efficiency [32].

In the same rat model as ours in the present study but immobilized up to 32 weeks, the posterior subintimal area of the experimental groups was smaller than that of the control groups through all the immobilization periods [1]. This result may reflect the decreased water and glycosaminoglycans of the SM. Our TEM observation showed that the space among collagen bundles and microfibrils was occupied with dense matrices in the experimental group, which may reflect the synovial atrophy due to decreased water content but not increased extracellular matrices. Further, adhesions of collagen bundles may limit lubrication and increase elasticity.

Previous studies analyzed the elasticity of the joint as a whole including ligament, capsule and SM with or without muscles [7,15,18,24]. But it was impossible to evaluate the elasticity of the individual arthrogenic components, especially of capsule and SM in those studies. The present study is the first that measured the elasticity of SM in situ by SAM in rat immobilized knees and revealed the increased elasticity of the posterior SM, subsequent to the inhibition of extension to cause the joint contracture. One reason why the elasticity is different between the anterior and the posterior SM of 8- and 16-week experimental group may be that compared with the posterior SM immobilized rigidly, the anterior SM keeps motion to a larger extent after immobilization with patella while being active. The present study suggested that the increased elasticity and structural changes of the posterior SM are one of the main causes of limited extension after immobilized in flexion.

Acknowledgements

The authors would like to acknowledge their valued input and efforts of Mr. Katsuyoshi Shoji, Mrs. Michiko Fukuyama and Miss Haruka Sasaki and thank Dr. Hans K Uhtoff and Dr. Guy Trudel for their technical advice of making the animal model.

References

1. Trudel G, Seki M, Uhthoff HK (2000) Synovial adhesions are more important than pannus proliferation in the pathogenesis of knee joint contracture after immobilization: an experimental investigation in the rat. J Rheumatol 27:351–357.
2. Patridge REH, Duthie JJR (1963) Controlled trial of the effect of complete immobilization of the joints in rheumatoid arthritis. Ann Rheum Dis 22:91–99.
3. Gault SJ, Spyker JM (1969) Beneficial effect of immobilization of joints in rheumatoid and related arthritis: A splint study using sequential analysis. Arthritis Rheum 12:34–44.
4. Peacock EE (1966) Some biochemical and biophysical aspects of joint stiffness: Role of collagen synthesis as opposed to altered molecular bonding. Ann Surg 164:1–12.

5. Damron TA, Greenwald TA, Breed A (1994) Chronological outcome of surgical tendoachilles lengthing and natural history of gastro-soleus contracture in cerebral palsy. Clin Orthop 301:249–255.
6. Trudel G. (1997) Differentiating the myogenic and arthrogenic components of joint contractures. An experimental study on the rat knee joint. Int J Rehabil Res 20:397–404.
7. Trudel G, Uhtoff HK (2000). Contractures secondary to immobility: is the restriction articular or muscular? An experimental longitudinal study in the rat knee. Arch Phys Med Rehabil 81:6–13.
8. Evans BE, Eggers GWN, Butler JK, Blumel J (1960) Experimental immobilization and remobilization of rat knee joints. J Bone Joint Surg 42A:737–758.
9. Amiel D, Akeson WH, Harwood FL, Mechanic GL (1980) The effect of immobilization on the types of collagen synthesized in periarticular connective tissue. Connect Tissue Res 8:27–32.
10. Enneking WF, Horowits M (1972) The intra-articular effects of immobilization on the human knee. J Bone Joint Surg 54A:973–985.
11. Hall MC (1963) Cartilage changes after experimental immobilization of the knee joint of the young rat. J Bone Joint Surg 45A:35–44.
12. Wilson PD (1944) Capsulectomy for the relief of flexion contractures of the elbow following fracture. J Bone Joint Surg 26A:71–86.
13. Wagner LC (1948) Fixed extension of the knee due to capsular contraction. NY State J Med 48:194–198.
14. Trudel G, Desaulniers N, Uhthoff HK, Laneuville O (2001) Different levels of COX-1 and COX-2 enzymes in synoviocytes and chondrocytes during joint contracture formation. J Rheumatol 28:2066–2074.
15. Trudel G, Uhthoff HK, Brown M (1999) Extent and direction of joint motion limitation after prolonged immobility: an experimental study in the rat. Arch Phys Med Rehabil 80:1542–1547.
16. Finsterbush A, Friedman B (1973) Early changes in immobilized rabbit knee joints: a light and electron microscopic study. Clin Orthop 92:305–319.
17. Roy S (1970) Ultrastructure of articular cartilage in experimental immobilization. Ann Rheum Dis 29:634–642.
18. Woo SL, Matthews JV, Akeson WH, Amiel D, Convery FR (1975) Connective tissue response to immobility: Correlative study of biomechanical measurements of normal and immobilized rabbit knees. Arthritis Rheum 18:257–264.
19. Hozumi N, Yamashita R, Lee CK, Nagao M , Kobayashi K, Saijo Y, Tanaka M, Tanaka N, Ohtsuki S (2004) Time-frequency analysis driven ultrasonic microscopy for biological tissue characterization. Ultrasonics 42:717–722.
20. Saijo Y, Tanaka M, Okawai H, Sasaki H, Nitta S, Dunn F (1997) Ultrasonic tissue characterization of infracted myocardium by scanning acoustic microscopy. Ultrasoud Med Biol 23:77–85.
21. Saijo Y, Sasaki H, Okawai H, Nitta S, Tanaka M (1998) Acoustic properties of atherosclerosis of human aorta obtained with high-frequency ultrasound. Ultrasound Med Biol 24:1061–1064.
22. Saijo Y, Jorgensen S, Mondek P, Sefranek V, Paaske W (2002) Acoustic inhomogeneity of carotid arterial plaques determined by GHz frequency range microscopy. Ultrasound Med Biol 28:933–937.
23. Sasano Y, Ohtani E, Narita K, Kagayama M, Murata M, Saito T, Shigenobu K, Takita H, Mizuno M, Kuboki Y (1993) BMPs Induce Direct Bone Formation in Ectopic Sites Independent of the Endochondral Ossification In Vivo. Anat Rec 236:373–380.
24. Shollmeier G, Sarkar K, Fukuhara K, Uhtoff HK (1996) Structural and functional changes in the canine shoulder after cessation of immobilization. Clin Orthop 323:310–315.
25. Schollmeier G, Uhtoff HK, Sarkar K, Furuhara K (1994) Effects of immobilization on the capsule of the canine glenohumeral joint. Clin Orthop 304:37–42.
26. Evans BE, Eggers GWN, Butler JK, Blumel J (1960) Experimental immobilization and remobilization of rat knee joints. J Bone Joint Surg 42A:737–758.
27. Enneking WF, Horowits M (1972) The Intra-articular effects of immobilization on the human knee. J Bone Joint Surg 54A:973–985.
28. Thaxter TH, Mann RA, Anderson CE (1965) Degeneration of immobilized knee joints in rats. J Bone Joint Surg 47A:567–585.
29. Hall MC (1963) Cartilage changes after experimental immobilization of the knee joint of the young rat. J Bone Joint Surg 45A:35–44.

30. Matsumoto F, Trudel G, Uhtoff HK (2002) High collagen type I and low collagen type III levels in knee joint contracture: an immunohistochemical study with histological correlate. Acta Orthop Scand 73:335–343.
31. Sood SC (1971) A study of the effects of experimental immobilization on rabbit articular cartilage. J Anat 108:497–507.
32. Akeson WH, Woo SL, Amiel D, Coutts RD, Daniel D (1973) The connective tissue response to immobility: biochemical changes in periarticular connective tissue of the immobilized rabbit knee. Clin Orthop 93:356–362.
33. Akeson WH, Amiel D and La Violette D (1968) The connective tissue response to immobility: An accelerated aging response? Exp Gerotol 3:289–301.

Corresponding author:
Yoshihiro Hagiwara
1-1 Seiryo-machi, Aoba-ku,
Sendai 980-8574, Japan
e-mail: hagi@mail.tains.tohoku.ac.jp
Tel: +81-22-717-7245
Fax: +81-22-717-7248

Ultrasonic Tissue Characterization of Atherosclerosis by a Speed-of-Sound Microscanning System

Yoshifumi Saijo, Esmeraldo Santos Filho, Hidehiko Sasaki, Tomoyuki Yambe, Motonao Tanaka, Naohiro Hozumi, *Member, IEEE*, Kazuto Kobayashi, and Nagaya Okada

***Abstract*—We have been developing a scanning acoustic microscope (SAM) system for medicine and biology featuring quantitative measurement of ultrasonic parameters of soft tissues. In the present study, we propose a new concept sound speed microscopy that can measure the thickness and speed of sound in the tissue using fast Fourier transform of a single pulsed wave instead of burst waves used in conventional SAM systems. Two coronary arteries were frozen and sectioned approximately 10 μm in thickness. They were mounted on glass slides without cover slips. The scanning time of a frame with 300 × 300 pixels was 90 s and two-dimensional distribution of speed of sound was obtained. The speed of sound was 1680 ± 30 m/s in the thickened intima with collagen fiber, 1520 ± 8 m/s in the lipid deposition underlying the fibrous cap, and 1810 ± 25 m/s in a calcified lesion in the intima. These basic measurements will help in the understanding of echo intensity and pattern in intravascular ultrasound images.**

I. Introduction

We have been developing a scanning acoustic microscopy (SAM) system for biomedical use since the 1980s [1]–[10]. We have been investigating the acoustic properties of various organs and disease states by using this SAM system. In the areas of medicine and biology, SAM has three main objectives. First, SAM is useful for intraoperative pathological examination because it does not require special staining. Second, SAM provides basic data for understanding lower-frequency medical ultrasound images such as in echocardiography or intravascular ultrasound. Third, SAM can be used to assess the biomechanics of tissues and cells at a microscopic level. The originality of the previous SAM system of Tohoku University lies in providing quantitative values of attenuation and speed of sound in thin slices of soft tissue. Although the system may still be in use, it was constructed using precise handcrafted technologies and analog signal acquisition circuits. In addition, the previous system needed repeated acquisitions for calculation of quantitative values because it used burst waves of different frequencies.

Recently, we proposed a prototype of a speed-of-sound microscanning system using a single pulsed wave instead of the burst waves used in conventional SAM systems [11]. In the present study, we constructed a compact speed-of-sound microscanning system and evaluated the system performance by measuring normal and atherosclerotic coronary arteries.

Manuscript received April 30, 2006; accepted October 18, 2006. This study was supported by Grants-in-Aid for Scientific Research (Scientific Research (B) 15300178, Scientific Research (B) 15360217) from the Japan Society for the Promotion of Science and Health and Labor Sciences Research Grants from the Ministry of Health, Labor and Welfare for the Research on Advanced Medical Technology (H17-Nano-001).

Y. Saijo, E. D. Santos Filho, H. Sasaki, T. Yambe, and M. Tanaka are with the Department of Medical Engineering and Cardiology, Institute of Development, Aging and Cancer, Tohoku University, Aobaku, Sendai 980-8575, Japan (e-mail: saijo@idac.tohoku.ac.jp).

N. Hozumi is with the Department of Electrical and Electronic Engineering, Aichi Institute of Technology, Yakusa, Toyota, 470-0392, Japan.

K. Kobayashi and N. Okada are with the Research and Development Headquarters, Honda Electronics Co. Ltd., Oiwa-cho, Toyohashi, 441-3193, Japan.

Digital Object Identifier 10.1109/TUFFC.2007.427

II. Methods

A. Principle of Acoustic Microscopy

In order to realize high-resolution imaging, the speed-of-sound microscanning system was designed to transmit and receive wide-frequency ultrasound up to 500 MHz. In our previous SAM system with burst waves, the central frequency was changed in 10-MHz steps between 100 and 200 MHz to obtain frequency-dependent characteristics of the amplitude and phase of the received signal. The spectrum for calculation of the thickness and sound speed of the material was approximated with the frequency-dependent characteristics. Fig. 1 shows an example of the frequency-dependent characteristics of the amplitude (a) and the phase (b).

Our previous SAM system was able to visualize quantitative acoustic properties of stable materials but it was not suitable for living biological materials because it required several measurements with different frequencies on the same position. Besides, the frequency range was not suitable for visualization of living cells because the spatial resolution was approximately 10 microns.

In the present method, a pulsed ultrasound with broadband frequency is captured in a time domain and the frequency domain analysis is performed by software. The data acquisition of each sampling point takes longer than with the conventional SAM, but only a single measurement on the observation plane is required in the proposed method.

First, considering the frequency characteristics of the high-frequency ultrasound transducer, the appropriate

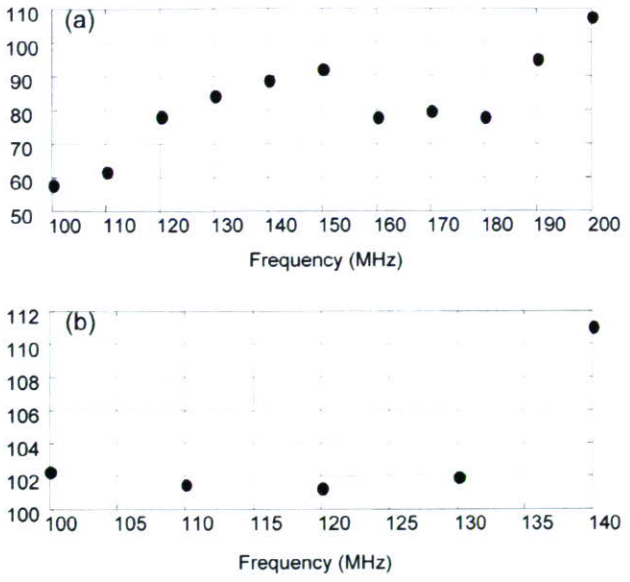

Fig. 1. Frequency-dependent characteristics of amplitude (a) and phase (b) obtained with our previous SAM system.

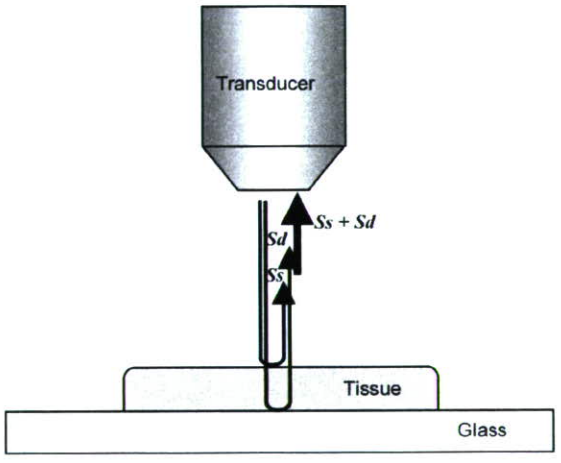

Fig. 2. Principle of quantitative measurement of acoustic properties by SAM.

pulse waveform and measurement system was designed. In order to analyze the signal in a frequency domain, the pulse width should be as short as possible and the pulse waveform should not contain many reverbs. Second, for realization of a compact system, integration of the scanner and signal acquisition was considered to design the whole acoustic microscope system.

Fig. 2 shows the principle of a scanning acoustic microscope. The soft biological material is attached to a substrate. Normal glass slides or high-molecular polymer materials used in dishes for cell culture can be used as the substrates. The biological material is sectioned at an appropriate thickness to separate the reflections from the tissue surface and from the interface between tissue and substrate. Single-layered cultured cells are also appropriate objects for SAM. The ultrasound is transmitted through a coupling medium and focused on the surface of the substrate. Transmitted ultrasound is reflected at both the surface of the biological material (S_s) and the interface between the biological material and the substrate (S_d). The transducer receives the sum of these two reflections. The interference of these two reflections is determined by the acoustic properties of the biological material. The determinants of the interference in the frequency (x-axis) are thickness and sound speed of the sample. The determinant of the interference of the intensity (y-axis) is the amplitude of the surface reflection and the attenuation of ultrasound propagating through the tissue. The concept of quantitative measurement of sound speed is based on the analysis of the interference frequency-dependent characteristics. In our previous SAM system, the frequency-dependent characteristics were obtained by serial measurements. The proposed sound speed SAM obtains the frequency-dependent characteristics by fast Fourier transform of a single broadband pulse.

B. Design of the Speed of Sound Microscanning System

An electric impulse was generated by a high-speed switching semiconductor. The start of the electric pulse was within 400 ps, the pulse width was 2 ns, and the pulse voltage was 40 V. Fig. 3(a) is the waveform of the electric pulse and Fig. 3(b) is the spectrum of the pulse. The spectrum extends to 500 MHz. The electric pulse was input to a transducer with a sapphire rod as an acoustic lens and with a central frequency of 300 MHz. Fig. 3(c) is the reflected wave form from the surface of the substrate. The ultrasonic pulse was changed from the electric pulse due to the frequency-dependent characteristics of the transducer, and it contained some oscillation components. The ultrasound spectrum is broad enough to cover 100–500 MHz [Fig. 3(d)].

The original electric pulse was almost an impulse, but the transmitted ultrasound contained oscillation components because of the thickness of the piezoelectric material of the transducer. The reflected wave also contained two components of reflections from the surface of the tissue and the interface between the tissue and the substrate. The waveform from the tissue and the glass was standardized by a reflection from the glass.

Fig. 3(e) shows the response to a singlet after this compensation. The reflections from the surface (front) and the interface (rear) are clearly seen in the waveform. These two peaks were separated by using proper window functions. The window function was originally a Gaussian function with 1 as its peak value, but the peak was flattened by splitting it at the peak point and inserting 1 with an appropriate length. Intensity and phase spectra of these separated waveforms were then calculated by Fourier transform.

Fig. 4 shows a block diagram of the speed-of-sound microscanning system for biological tissue characterization. A single ultrasound pulse with a pulse width of 2 ns was emitted and received by the same transducer above the specimen. The aperture diameter of the transducer was

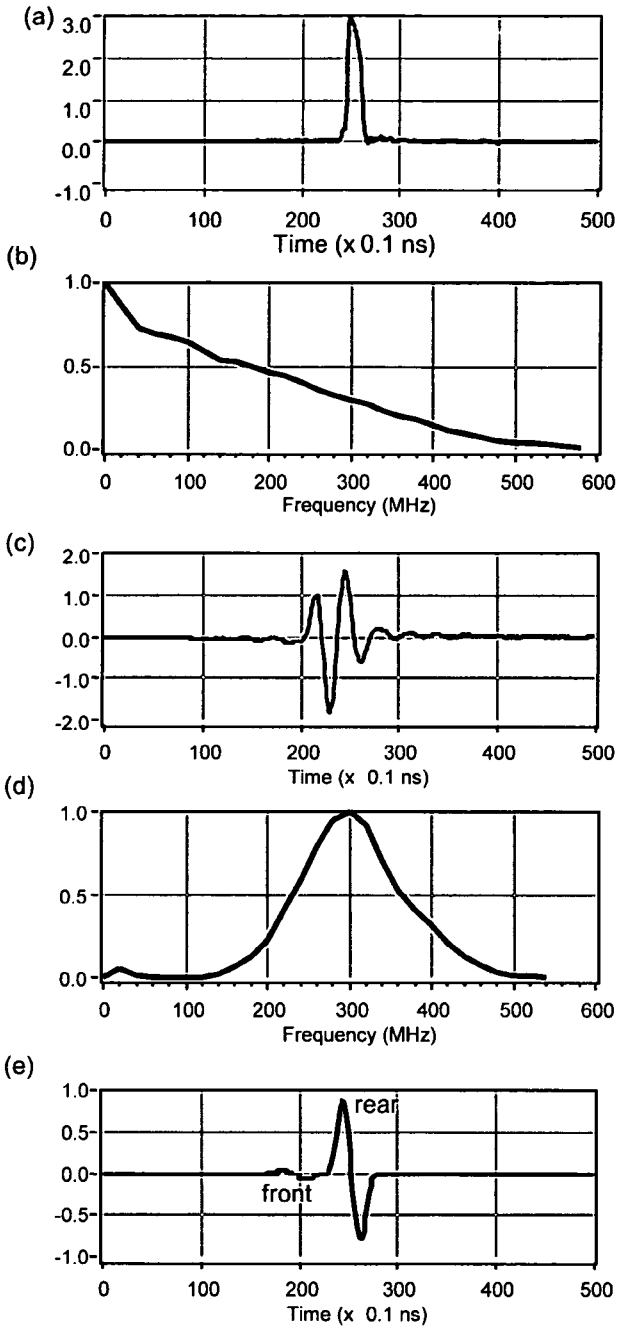

Fig. 3. (a) Waveform of the electric pulse; (b) the spectrum of the pulse; (c) the reflected wave form from the surface of the substrate; (d) ultrasound spectrum of the transducer; and (e) response to a singlet after standardization by a reflection from the glass. The reflections from the tissue surface (front) and the interface between the tissue and glass (rear) were separated in (e). The y-axis of each figure is normalized intensity (arbitrary units).

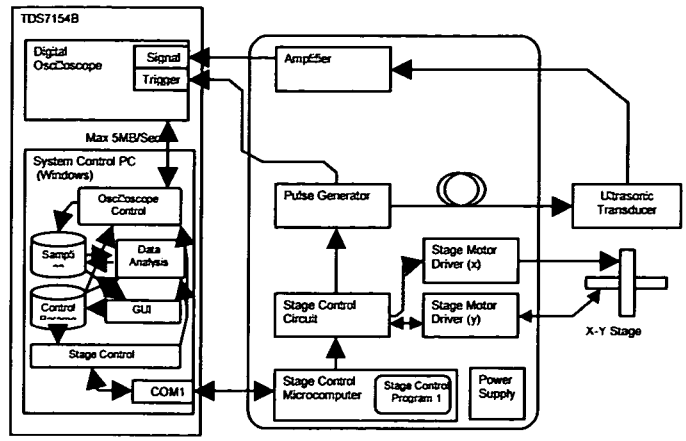

Fig. 4. Block diagram of sound speed microscopy.

1.2 mm, and the focal length was 1.5 mm. The central frequency was 300 MHz, the bandwidth was 100–500 MHz, and the pulse repetition rate was 10 kHz. The diameter of the focal spot was estimated to be 6.5 μm at 500 MHz by taking into account the focal distance and the sectional area of the transducer. Saline was used as the coupling medium between the transducer and the specimen. The reflections from the tissue surface and those from the interface between the tissue and glass were received by the transducer and were introduced into a Windows-based PC (Pentium D, 3.0 GHz, 2GB RAM, 250GB HDD) via a digital oscilloscope (Tektronix TDS7154B, Beaverton, OR). The frequency range was 1 GHz, and the sampling rate was 20 GS/s. Four consecutive values of the time taken for a pulse response were averaged in order to reduce random noise.

The transducer was mounted on an X-Y stage with a microcomputer board that was driven by the PC through an RS-232C interface. Both the X-scan and the Y-scan were driven by linear servo motors and the position was detected by an encoder. The scan was controlled to reduce the effects of acceleration at the start and deceleration at the end of the X-scan. Finally, two-dimensional distributions of ultrasonic intensity, speed of sound, attenuation coefficient, and thickness of a specimen measuring 2.4 × 2.4 mm were visualized using 300 × 300 pixels. The total scanning time was 90 s.

C. Signal Analysis

Denoting the standardized phase of the reflection wave at the tissue surface as ϕ_{front}, and the standardized phase at the interference between the tissue and the substrate as ϕ_{rear},

$$2\pi f \times \frac{2d}{c_o} = \phi_{\text{front}}, \tag{1}$$

$$2\pi f \times 2d\left(\frac{1}{c_o} - \frac{1}{c}\right) = \phi_{\text{rear}}, \tag{2}$$

where d is the tissue thickness, c_o is the sound speed in coupling medium, and c is the sound speed in the tissue.

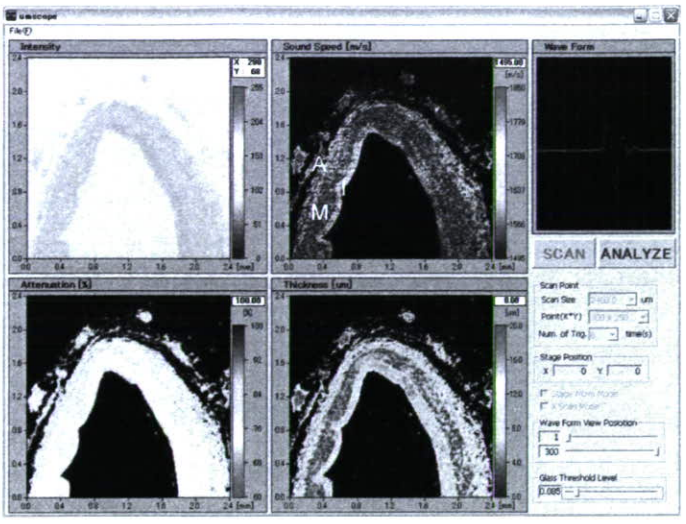

Fig. 5. PC window of speed of sound microscopy showing a normal coronary artery. Upper left: amplitude image; upper right: speed of sound image; lower left: attenuation image; and lower right: thickness. I: Intima; M: media; A: adventitia.

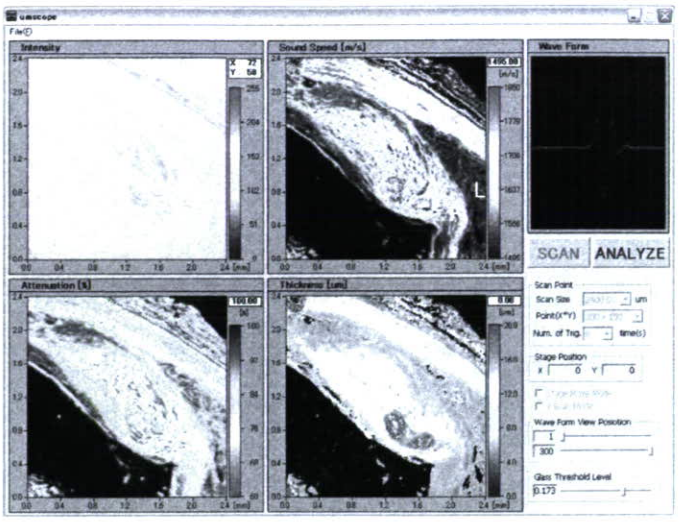

Fig. 6. PC window of speed-of-sound microscopy showing an atherosclerotic coronary artery. Upper left: amplitude image; upper right: speed of sound image; lower left: attenuation image; and lower right: thickness. I: intima; C: calcified lesion; F: fibrous cap; L: lipid.

Thickness is obtained as

$$d = \frac{c_o}{4\pi f}\phi_{\text{front}}. \tag{3}$$

Finally, sound speed is calculated as

$$c = \left(\frac{1}{c_o} - \frac{\phi_{\text{rear}}}{4\pi f d}\right)^{-1}. \tag{4}$$

After determination of the thickness, attenuation of ultrasound was then calculated by dividing the amplitude by the thickness and the frequency.

D. Tissue Preparation

Normal and atherosclerotic human coronary arteries were obtained from autopsy. The specimens were rinsed in phosphate buffer saline (PBS) and immersed in 10% to 30% sucrose solutions. Then the specimens were embedded in optimal cutting temperature (OCT) compound and rapidly frozen by liquid nitrogen at −20°C. The specimens were sliced at approximately 10 microns by a cryostat and mounted on silane-coated glass slides.

III. Results

Fig. 5 shows a PC window of the speed-of-sound microscanning system. The upper left is an intensity image, the upper right is a sound speed image, the lower left is an attenuation image, and the lower right is the thickness distribution of the normal coronary artery. In the present case, the attenuation image of the system means the intensity divided by the thickness. It is not quantitatively calculated as the attenuation coefficient. The intima was thin, and the sound speed was 1600 ± 20 m/s in the intima (I), 1560 ± 18 m/s in the medium (M), and 1590 ± 22 m/s in the adventitia (A). The thickness was 7.2 ± 0.1 μm in the intima, 4.8 ± 0.2 μm in the medium and 7.2 ± 0.1 μm in the adventitia. In qualitative analysis, the attenuation of the medium was slightly lower than that of either the intima or the adventitia.

Fig. 6 is an atherosclerotic coronary artery. The sound speed was 1680 ± 30 m/s in the thickened intima (I) with collagen fiber, 1520 ± 8 m/s in lipid deposition (L) underlying the fibrous cap (F), and 1810 ± 25 m/s in the calcified lesion (C) in the intima. The thickness was 11.8 ± 0.1 μm in the intima, 11.6 ± 0.2 μm in the medium and 14.8 ± 0.1 μm in the lipid deposition. In qualitative analysis, the attenuation of the calcified lesion was high and the attenuation in lipid deposition was low.

IV. Discussion

In the present study, speed of sound in the excised human coronary arteries was measured with the specially developed microscanning system. The results showed that the speed of sound in the intima and the adventitia, mainly consisting of collagen fiber, had higher values than that of the medium, mainly consisting of vascular smooth muscle. The difference of acoustic properties may lead to the classical three-layered appearance of a normal coronary artery in clinical intravascular ultrasound (IVUS) imaging. The findings indicate that the echo intensity is determined by the difference of acoustic impedance between neighboring layers because the specific acoustic impedance is the product of the speed of sound and the density. The distribution and the structure of materials with different acoustic properties may also contribute to the echo pattern in IVUS imaging.

The thick fibrous cap, consisting of collagen fiber in an atherosclerotic plaque, showed higher values of speed of

sound and attenuation than did normal medium. Generally, absorption and scattering are the two main factors of attenuation of ultrasound. Thus, the high scattering within the thickened intima or calcified lesion may lead to the high intensity echo in the clinical IVUS imaging. The region of lipid deposition showed low values of speed of sound. These values explain the low echo in the same manner as for renal cysts containing water-like fluid. Besides the absolute low values, the homogeneity of acoustic properties within the lipid pool may lead to the low scattering and consequently a lipid pool shows a low-intensity echo.

As ultrasound has the character of an elastic wave, ultrasound itself is closely related to the mechanical properties of tissues. The sound speed in a solid medium may be taken as

$$c = \sqrt{\frac{E(1-\sigma)}{\rho(1+\sigma)(1-2\sigma)}} \cdots, \tag{5}$$

where c is the speed of sound, E is the Young's elastic modulus, ρ is the density, and σ is the Poisson's ratio. The Poisson's ratio in biological soft materials is assumed to be nearly 0.5 and the density of these vary 3% [4]. Although these simple assumptions are not to be applied precisely, the information on the relative two-dimensional elasticity distribution can be assessed by sound speed image. A high value of sound speed means high elasticity of collagen which is the main component of the intimal thickening. Lipid is the main component of the lucent echogeneicity plaque, and the elasticity is low. The present study proved that the tissue component in the "hard plaque" was really hard and the component of "soft plaque" was really soft. Also, the intima mainly consisting of fibrotic tissues was harder than the normal intima-medium complex. The difference in the elasticity may explain why intimal tear often occurred at the junction of the thinnest plaque and adjacent normal arterial wall [12], [13]. Acoustic microscopy imaging, especially the sound speed image, is the interpretation of elasticity mapping, and it may also help in the understanding of the "elastography" [14] imaging of atherosclerotic plaques from a mechanical point of view.

There have been some time-resolved acoustic microscope systems [15], [16]. The most important feature of our sound speed microscope is that the system calculates the speed of sound and the thickness by frequency-domain analysis of the interference between the reflections from the tissue surface and from the interface between the tissue and glass. However, the error of the sound speed value is 15 m/s by the algorithm [17]. Besides, the system is not able to measure the speed of sound when the surface reflection is weak or the thickness is thinner than 3 μm because the two reflections cannot be separated.

V. Conclusions

An acoustic microscope system that can measure the sound speed of thin slices of biological material was developed. It is a unique acoustic microscope because it uses a single pulse and the Fourier transform to calculate the sound speed and the thickness at all measuring points. Although the data acquisition time of a single frame was greater than that in conventional SAM, the total time required for calculation was significantly shorter. The acoustic microscope system can be applied to intraoperative pathological examination, basic data for understanding lower-frequency medical ultrasound images, and assessment of biomechanics of tissues and cells at a microscopic level.

References

[1] M. Tanaka, H. Okawai, N. Chubachi, J. Kushibiki, and T. Sannomiya, "Propagation properties of ultrasound in acoustic microscopy through a double-layered specimen consisting of thin biological tissue and its holder," *Jpn. J. Appl. Phys.*, vol. 23, pp. 197–199, 1984.

[2] Y. Saijo, M. Tanaka, H. Okawai, and F. Dunn, "The ultrasonic properties of gastric cancer tissues obtained with a scanning acoustic microscope system," *Ultrasound Med. Biol.*, vol. 17, pp. 709–714, 1991.

[3] H. Sasaki, M. Tanaka, Y. Saijo, H. Okawai, Y. Terasawa, S. Nitta, and K. Suzuki, "Ultrasonic tissue characterization of renal cell carcinoma tissue," *Nephron*, vol. 74, pp. 125–130, 1996.

[4] Y. Saijo, M. Tanaka, H. Okawai, H. Sasaki, S. Nitta, and F. Dunn, "Ultrasonic tissue characterization of infarcted myocardium by scanning acoustic microscopy," *Ultrasound Med. Biol.*, vol. 23, pp. 77–85, 1997.

[5] Y. Saijo, H. Sasaki, H. Okawai, S. Nitta, and M. Tanaka, "Acoustic properties of atherosclerosis of human aorta obtained with high-frequency ultrasound," *Ultrasound Med. Biol.*, vol. 24, pp. 1061–1064, 1998.

[6] Y. Saijo, H. Sasaki, M. Sato, S. Nitta, and M. Tanaka, "Visualization of human umbilical vein endothelial cells by acoustic microscopy," *Ultrasonics*, vol. 38, pp. 396–399, 2000.

[7] Y. Saijo, T. Ohashi, H. Sasaki, M. Sato, C. S. Jorgensen, and S. Nitta, "Application of scanning acoustic microscopy for assessing stress distribution in atherosclerotic plaque," *Ann. Biomed. Eng.*, vol. 29, pp. 1048–1053, 2001.

[8] H. Sasaki, Y. Saijo, M. Tanaka, and S. Nitta, "Influence of tissue preparation on the acoustic properties of tissue sections at high frequencies," *Ultrasound Med. Biol.*, vol. 29, pp. 1367–1372, 2003.

[9] Y. Saijo, T. Miyakawa, H. Sasaki, M. Tanaka, and S. Nitta, "Acoustic properties of aortic aneurysm obtained with scanning acoustic microscopy," *Ultrasonics*, vol. 42, pp. 695–698, 2004.

[10] H. Sano, Y. Saijo, and S. Kokubun, "Material properties of the supraspinatus tendon at its insertion—A measurement with the scanning acoustic microscopy," *J. Musculoskeletal Res.*, vol. 8, pp. 29–34, 2004.

[11] N. Hozumi, R. Yamashita, C. K. Lee, M. Nagao, K. Kobayashi, Y. Saijo, M. Tanaka, N. Tanaka, and S. Ohtsuki, "Time-frequency analysis for pulse driven ultrasonic microscopy for biological tissue characterization," *Ultrasonics*, vol. 42, pp. 717–722, 2004.

[12] R. T. Lee and R. D. Kamm, "Vascular mechanics for the cardiologist," *J. Amer. Coll. Cardiol.*, vol. 23, pp. 1289–1295, 1994.

[13] A. Maehara, G. S. Mintz, A. B. Bui, M. T. Castagna, O. R. Walter, C. Pappas, E. E. Pinnow, A. D. Pichard, L. F. Satler, R. Waksman, W. O. Suddath, J. R. Laird , Jr., K. M. Kent, and N. J. Weissman, "Incidence, morphology, angiographic findings, and outcomes of intramural hematomas after percutaneous coronary interventions: An intravascular ultrasound study," *Circulation*, vol. 105, pp. 2037–2042, 2002.

[14] C. L. de Korte, G. Pasterkamp, A. F. van der Steen, H. A. Woutman, and N. Bom, "Characterization of plaque components with intravascular ultrasound elastography in human femoral and coronary arteries in vitro," *Circulation*, vol. 102, pp. 617–623, 2002.

[15] C. M. Daft and G. A. Briggs, "The elastic microstructure of various tissues," *J. Acoust. Soc. Amer.*, vol. 85, pp. 416–422, 1989.
[16] A. F. van der Steen, M. H. Cuypers, J. M. Thijssen, and P. C. de Wilde, "Influence of histochemical preparation on acoustic parameters of liver tissue: A 5-MHz study," *Ultrasound Med. Biol.*, vol. 17, pp. 879–891, 1991.
[17] N. Hozumi, "Development of sound speed acoustic microscopy for biological nano-imaging by picosecond evoked ultrasonic pulse," Research Accomplishment Report of Grants-in-aid for Scientific Research, 2006. (in Japanese)

Yoshifumi Saijo was born in Yokohama, Japan, on July 21, 1962. He received the M.D. and the Ph.D. degrees in 1988 and 1993, respectively, from Tohoku University.

He is currently an associate professor in the Department of Medical Engineering and Cardiology at the Institute of Development, Aging and Cancer, Tohoku University, and the Department of Cardiovascular Surgery, Tohoku University Hospital. His main research interests are assessment of biomechanics of cells and tissues by high-frequency ultrasound and clinical ultrasonic evaluation of cardiovascular system with intravascular ultrasound and transesophageal echocardiography. He received an award in 1997 for his outstanding research paper in *Ultrasound in Medicine and Biology*, the official journal of the World Federation of Ultrasound in Medicine and Biology. He is a member of the Japan Society of Ultrasonics in Medicine, the Japanese Society of Echocardiography, and the Japan Circulation Society.

Esmeraldo dos Santos Filho was born in 1971 in Sao Luis - MA, Brazil. He earned his bachelor and master degrees at the Federal University of Maranhao, in Brazil, in the years 1998 and 2000, respectively. In 2005, he earned his Ph.D. degree at Tohoku University in Japan.

During the academic year of 2001, he worked as a lecturer on digital systems at the Department of Electrical Engineering of the Federal University of Maranhao. Currently, he is a postdoctoral fellow of the Japan Association for Advancement of Medical Equipment at the Institute of Development, Aging, and Cancer, Tohoku University. His fields of interest are applications of artificial intelligence in biomedical image and signal processing. He is a member of the IEEE Signal Processing Society.

Hidehiko Sasaki received his M.D. degree from Yamagata University in 1990 and his Ph.D. degree from Tohoku University in 1996. He is currently Director of the Department of Cardiology at Miyagi Cardiovascular and Respiratory Center. His main research interest is acoustic microscopy evaluation of renal and cardiovascular diseases. He is a member of the Japan Society of Ultrasonics in Medicine and the Japanese Society of Interventional Cardiology.

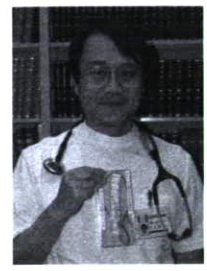

Tomoyuki Yambe was born in May 7, 1959 in Sendai, Japan. He received the M.D. and the Ph.D. degrees in 1985 and 1989, respectively, from Tohoku University.

He is currently a professor in the Department of Medical Engineering and Cardiology at the Institute of Development, Aging and Cancer, Tohoku University. His main research interest includes development of artificial organs. He is a member of the Japanese Society for Artificial Organs.

Motonao Tanaka was born in Tokyo, Japan, on January 1, 1932. He received the M.D. and the Ph.D. degrees in 1958 and 1962, respectively, from Tohoku University. He was a professor in the Department of Medical Engineering and Cardiology at the Institute of Development, Aging and Cancer, Tohoku University from 1984 to 1996. He is currently Director of the Japan Anti-tuberculosis Association of Miyagi Prefecture. He invented one of the world's first B-mode echocardiographs in the early 60s. Since then he has been contributing to the development of medical ultrasound. He started developing acoustic microscopy for medicine and biology in 1985 and his current interest is "echodynamography" which enables visualization of stream lines and dynamic pressure distribution in heart chambers. He is a member of the Japan Society of Ultrasonics in Medicine, the Japanese Society of Echocardiography, and the Japan Circulation Society.

Naohiro Hozumi (M'94) was born in Kyoto, Japan, on April 2, 1957. He received his B.S., M.S., and Ph.D. degrees in 1981, 1983, and 1990, respectively, from Waseda University. He was employed at the Central Research Institute of Electric Power Industry (CRIEPI) from 1983 to 1999. He was an associate professor at Toyohashi University of Technology from 1999 to 2006. Since 2006, he has been a professor at Aichi Institute of Technology.

He has been engaged in research on insulating materials and diagnosis for high-voltage equipment, acoustic measurement for biological and medical applications, etc. He received awards in 1990 and 1999 from the IEE of Japan for his outstanding research papers. He is a member of IEEE, IEE of Japan, and the Acoustic Society of Japan.

Kazuto Kobayashi was born in Aichi, Japan, on June 8, 1952. He received his B.S. degree in electrical engineering from Shibaura Institute of Technology, Tokyo, Japan, in 1976.

He is currently Director of the Department of Research and Development at Honda Electronics Co. Ltd., Toyohashi, Japan. His research activities and interests include medical ultrasound imaging, signal processing, and high-frequency ultrasound transducers.

Nagaya Okada was born in Aichi, Japan, on January 27, 1964. He received the B.S. degree in electrical engineering from Shizuoka University, Shizuoka, Japan, in 1987, and the M.S. and Ph.D. degrees in electrical engineering from Shizuoka University, Shizuoka, Japan, in 1990 and 1993, respectively.

He is currently a manager of the Department of Research and Development at Honda Electronics Co. Ltd., Toyohashi, Japan. His research activities and interests include digital signal processing, ultrasound imaging and high-frequency ultrasound transducers.

Proceedings of the 29th Annual International
Conference of the IEEE EMBS
Cité Internationale, Lyon, France
August 23-26, 2007.

Blood Flow Visualization of Left Atrial Spontaneous Echo Contrast (SEC) Using gradient based optical flow estimation

Akira Tanaka, *Member, IEEE*, Yoshifumi Saijo, *Member, IEEE*

Abstract— **Left atrial spontaneous echo contrast (SEC) is a dynamic smoke-like signal caused by an increased ultrasonic backscatter from aggregation of the cellular components of blood in the conditions of blood stases or low-velocity blood flow. SEC can be detected by transesophageal echocardiography (TEE). SEC has been proposed as an important cadioembolic source in patients with nonrheumatic arial fibrillation. Previous clinical investigations have shown that the presence of SEC is associated with a greater incidence of left atrial thrombi. Usually, the blood flow velocity is slower than lower limit of Doppler method in SEC. In order to diagnose SEC quantitatively, blood flow visualization in left atrium was performed using gradient based optical flow estimation.**

A movie of left atrium (LA) with SEC in a patient with atrial fibrillation was recorded by TEE with the frequency range of 4-7.5 MHz. Serial still frames were made from the movie. The 2-D flow vector map was calculated from consecutive frame images using gradient based optical flow estimation.

In the result of 2-D blood flow vector map, the low and swirling flow in LA were successfully visualized.

I. Introduction

LEFT atrial spontaneous echo contrast (SEC) is a dynamic smoke-like signal (Fig. 1). It caused by an increased ultrasonic backscatter from aggregation of the cellular components of blood in the conditions of blood stases or low-velocity blood flow [1][2]. SEC can be detected by transesophageal echocardiography (TEE). The most common condition predisposing to left atrial SEC are atrial fibrillation (AF) and mitral stenosis. Hence, SEC has been proposed as an important cardioembolic source in patients with nonrheumatic atrial fibrillation [1]-[3]. Previous clinical investigations have shown that the presence of SEC is associated with a greater incidence of left atrial thrombi [4][5]. Therefore, it is very important to diagnosis SEC in order to reduce the risk of thromboembolism. However, SEC is still described qualitatively [6][7].

The assessment of thromboembolic risk by measurement of left atrium (LA) appendage velocities using pulsed Doppler imaging during TEE in atrial fibrillation has become accepted [8]. LA appendage velocity may also represent LA appendage contractile function. Some studies have suggested that the conversion from atrial fibrillation to sinus rhythm may be predicted by evaluating LA appendage velocities before cardioversion [9]. Quantitative blood flow analysis in echocardiography has been mainly addressed using Doppler method. This approach, however, have disadvantages for SEC analysis. It has angle dependency because it only measures the velocity throughout the ultrasound beam direction. Besides, it cannot measure the low blood flow velocity which is slower than lower limit of Doppler method. Hence, it is difficult to visualize the swirling blood flow in left atrium (LA).

The aim of this study is visualization of retardant flow vector in LA.

Fig. 1. Spontaneous echo contrast of left atrium in transesophageal echocardiography

II. Methods

A. Clinical Data Acquisition

Transesophageal echocardiography was performed in a 70-year-old man with atrial fibrillation using a color Doppler system (SONOS5500, Philips, USA) and a 4-7.5MHz multiplane transducer (Omniplane 2, Hewlett Packerd, USA) under stable general anesthesia.

SEC was identified as a dynamic smokelike signal that swirled slowly in a circular pattern in the left atrium. The

Manuscript received April 16, 2007. This work was supported by Grants from New Energy and Industrial Technology Development organization (06001905-0)

Akira Tanaka is with Faculty of Symbiotic System Science, Fukushima University, Kanayagawa 1, Fukushima 960-1296, Japan. (e-mail: a-tanaka@ieee.org)

Yoshifumi Saijo is with Institute of Development, Aging and Cancer, Tohoku University, Seiryo-cho 4-1, Aoba-ku, Sendai 980-8575, Japan.

1-4244-0788-5/07/$20.00 ©2007 IEEE